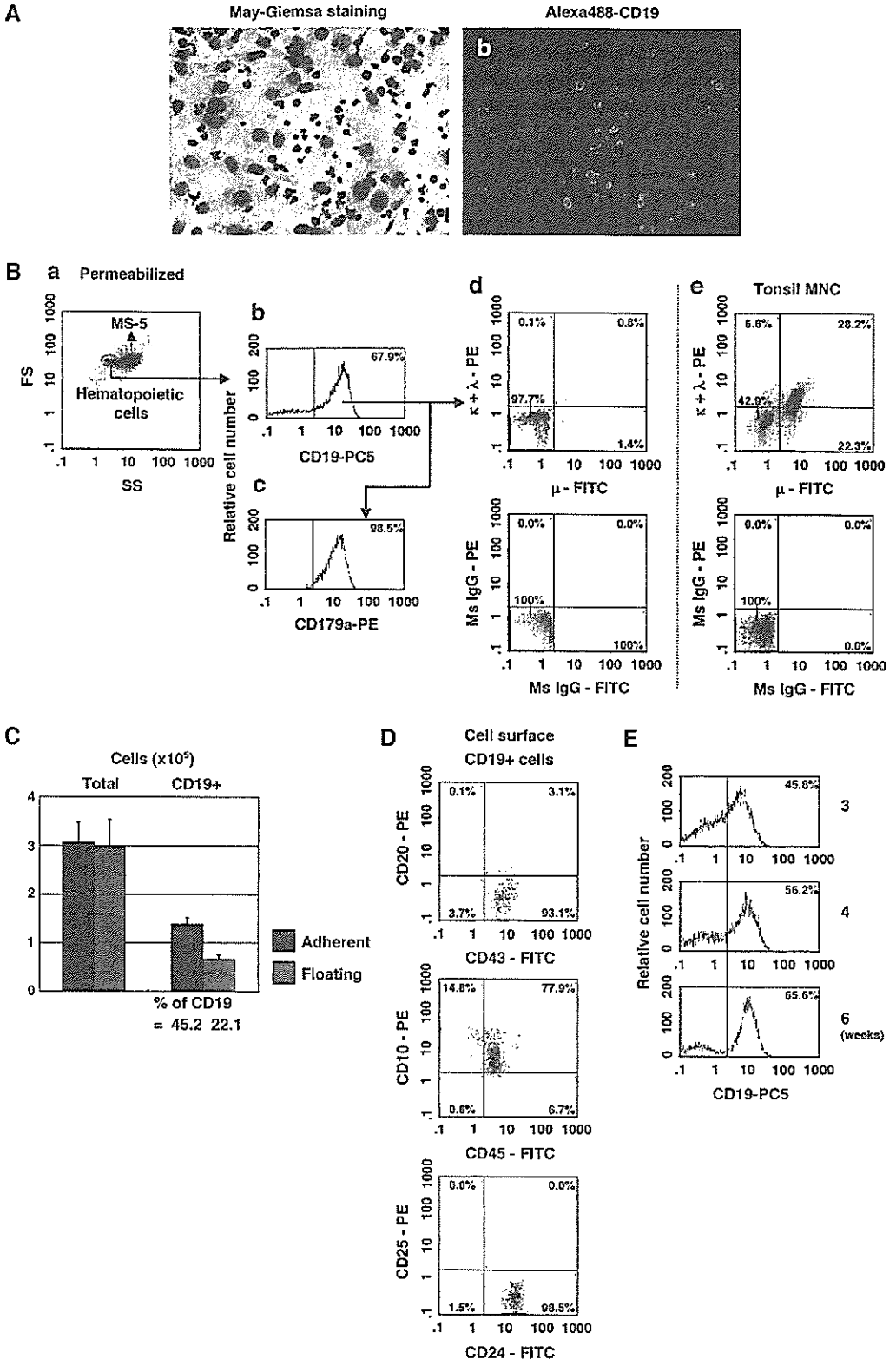
A
May-Giemsa staining
Alexa488-CD19
B a Permeabilized
MS-5
Hematopoietic cells
FS
SS
b
CD19-PC5
Relative cell number
67.9%
c
CD179a-PE
98.5%
d
κ+λ - PE
μ - FITC
Ms IgG - PE
Ms IgG - FITC
0.1%
0.8%
97.7%
1.4%
0.0%
100%
e Tonsil MNC
6.6%
28.2%
42.0%
22.3%
C
Cells (x10⁵)
Total
CD19+
Adherent
Floating
% of CD19
= 45.2 22.1
D
Cell surface
CD19+ cells
CD20 - PE
CD43 - FITC
CD10 - PE
CD45 - FITC
CD25 - PE
CD24 - FITC
3.1%
3.7%
93.1%
14.8%
77.9%
0.6%
6.7%
1.5%
98.5%
E
45.8%
56.2%
65.6%
3
4
6
(weeks)
CD19-PC5

culture supernatants of MS-5 cells was determined by sandwich enzyme-linked immunosorbent assay (ELISA), using Mouse IGF-I Quantikine ELISA Kit (R&D Systems, Wiesbaden, Germany), according to manufacturer's instruction. Experiments were performed in triplicate, and mean ± SDs of cell numbers are shown in Figure 2C.

Results

Differentiation of pro-B cells from human BM CD34$^+$ cells by coculturing with murine stromal MS-5 cells

Murine stromal cell line MS-5 has been reported to possess the capability to support differentiation of B-lineage cells from human cord blood (CB) CD34$^+$ cells [14–17]. Coincident with these previous reports, we observed that human BM CD34$^+$ cells generated a high number of CD19$^+$ B cells after cocultivation with MS-5 cells (Fig. 1A and B). Starting with 4×10^4 CD34$^+$ cells, approximately 0.4 to 1.3×10^6 mononuclear cells, 30.1% to 68.2% of which were CD19$^+$ cells, were obtained after 4 weeks of cultivation. As shown in Figure 1C, approximately half of the hematopoietic cells were floating, while the remainder were adhered to the MS-5 cells and the CD19$^+$ cells were more abundant in adherent cell fraction.

As shown in Figure 1B, most of the CD19$^+$ B cells obtained after 9 weeks of cultivation expressed cytoplasmic CD179a. The CD179a is reported to be already expressed in pro-B cells, remains expressed on B-cell precursors, and disappears upon differentiation from pre-B cells to mature B cells [9]. In contrast, a few percent of CD19$^+$ cells were positive for surface and/or cytoplasmic μ heavy chain and a portion of them expressed either the κ or λ light chains (Fig. 1B). We also observed that CD10, CD24, CD43, and CD45 were expressed but CD20 and CD25 were not in the CD19$^+$ cells (Fig. 1D). No difference in immunophenotypic characteristics was observed between the CD19$^+$ cells in adherent cell fraction and that in floating cell fraction (data not shown). Based on the above data, we concluded that human BM CD34$^+$ cells can differentiate into pro-B cells, but not into pre-B cells, after coculturing with the murine stromal cell line MS-5 in the present culture system. CD19$^+$ cells cultured for 4 weeks were also examined, and similar immunophenotypic characteristics were noted (data not shown).

Next, we examined the time course of the expression of CD19 in human BM CD34$^+$ cells in our culture system. CD19$^+$ cells were already detected after 1 week of culture (data not shown), and the number of CD19$^+$ cells increased throughout the course of the cell culture thereafter. After 4 to 9 weeks of culture, both the fluorescent intensity of CD19 on each cell and the percentage of CD19$^+$ cells out of the total number of cells continued to increase (Fig. 1E), but the total number of CD19$^+$ cells did not change significantly (data not shown). When expression of transcription factors related to early B-cell differentiation was analyzed by RT-PCR, expression profiles of these factors were well correlated with proliferation of CD19$^+$ cells as described (data not shown). Therefore, pro–B-cell development after 4 weeks of culture in the present system was analyzed in the following experiments.

Effect of IGF-I on in vitro human pro–B-cell development

Because expression of IGFRs in cultured CD34$^+$ BM cells was detected (Fig. 2A), we first tested the effect of adding exogenous recombinant human IGF-I to the coculture of CD34$^+$ BM cells and MS-5 cells to evaluate the contribution of IGF-I to human pro–B-cell development; no significant change in pro–B-cell development was observed (data not shown).

However, RT-PCR analysis revealed expression of IGF-I in MS-5 cells (Fig. 2B). Results of ELISA further demonstrated that mouse IGF-I was indeed secreted in the culture supernatant of MS-5 cells (Fig. 2C). As presented in Figure 2D, mouse IGF-I is active in human hematopoietic cells and can induce tyrosine-phosphorylation of human IGF-IR expressed on NALM-16 cells derived from human B-precursor acute lymphoblastic leukemia. When we tested similarly, MS-5 culture supernatant could stimulate IGF-IR on NALM-16 cells, whereas freshly prepared medium containing 10% FCS could not, indicating that mouse IGF-I secreted from MS-5 cells is sufficient to stimulate

Figure 1. Characterization of human bone marrow (BM) CD34$^+$ cells cocultured with murine stromal cells. (**A**) Human BM CD34$^+$ cells were cocultured for 4 weeks with murine stromal MS-5 cells on cover slips. At the end of the culture period, the cells were examined with either May-Grünwald-Giemsa staining (**a**) or CD19 immunostaining (green) with nuclear counter staining by 4′,6-diamidino-2-phenylindole (blue) (**b**). Original magnification ×400. (**B**) Human BM CD34$^+$ cells cocultured for 9 weeks with MS-5 cells were harvested. The expression of cell surface CD19, κ/λ light chains and cytoplasmic CD179a and μ heavy chain was simultaneously assessed by flow cytometry with cell-permeabilization technique as described in Materials and Methods. In cultured BM cells (**a**), CD19$^+$ cells were gated (**b**), and expression of CD179a (**c**), μ heavy chain, and κ/λ light chains (**d**) was examined. As a negative control, same sample specimen stained with isotype-matched control mouse IgG was also presented. As a positive control, mononuclear cells prepared from tonsil were similarly treated as in (**d**) and presented (**e**). FITC = fluorescein isothiocyanate; FS = forward light scatter; SS = side light scatter. (**C**) Human BM CD34$^+$ cells were cocultured with MS-5 cells for 4 weeks and the adherent cell fraction and floating cell fraction were collected separately. Total cell number and expression of CD19 were examined as above. (**D**) Human BM CD34$^+$ cells were cocultured with MS-5 cells as in (**B**), and multicolor immunofluorescence study was performed as above. CD19$^+$ cells were gated, and expression of surface B-cell differentiation markers, as indicated, was examined using flow cytometry. (**E**) Human BM CD34$^+$ cells were cocultured with MS-5 cells for 3, 4, and 6 weeks, and expression of CD19 was examined using flow cytometry.

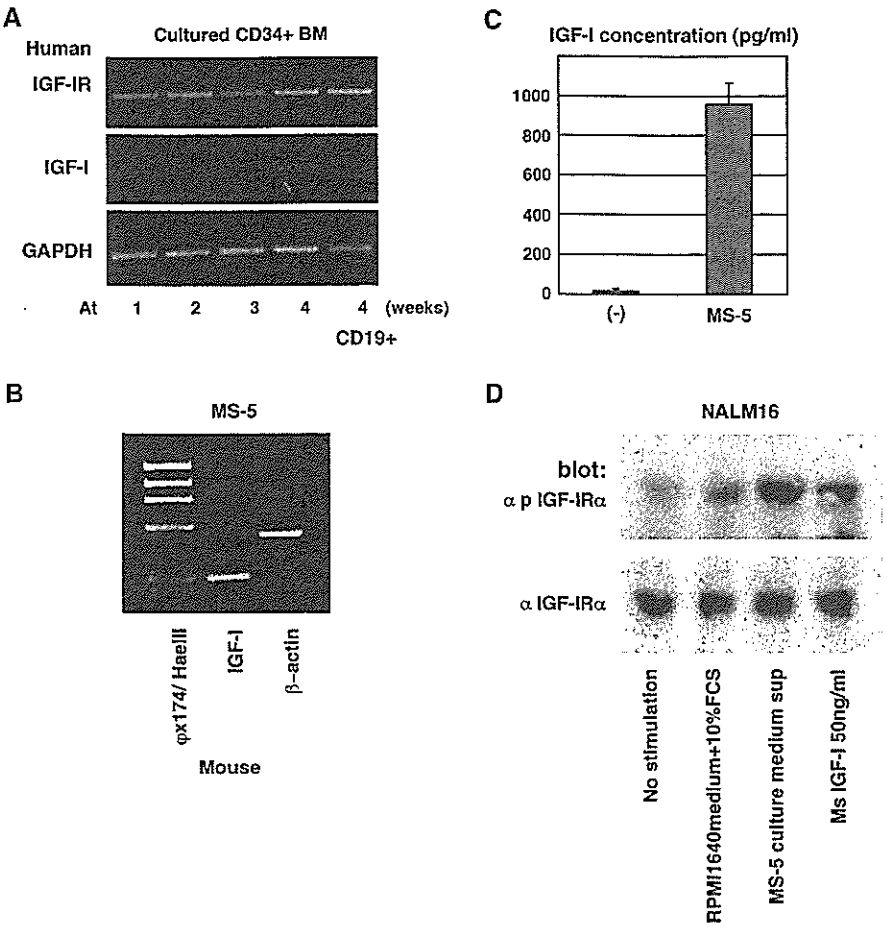

Figure 2. Expression of insulin-like growth factors (IGFs) and IGF receptors on cultured human bone marrow (BM) $CD34^+$ cells and murine stromal MS-5 cells. (**A**) Human BM $CD34^+$ cells were cocultured with MS-5 cells for 1, 2, 3, or 4 weeks, as shown in Figure 1. At the end of the culture periods, the floating fraction of the cultured human BM cells was collected and expression of human IGF-I receptor (IGF-IR) and IGF-I was examined using reverse transcriptase polymerase chain reaction (RT-PCR). As an internal control, expression of human glyceraldehyde phosphate dehydrogenase was also examined. $CD19^+$ cells were sorted from 4-week cultured human BM $CD34^+$ cells and similarly examined ($CD19^+$). (**B**) Expression of mouse IGF-I in MS-5 cells was examined using RT-PCR. As an internal control, expression of mouse β-actin was also examined. The $\phi\chi174/HaeIII$ molecular weight marker was presented in the left side. (**C**) MS-5 cells were cultured alone for 4 weeks and the culture supernatant was collected. Subsequent concentration of mouse IGF-I secreted by MS-5 cells in culture supernatant was determined by enzyme-linked immunosorbent assay. As a negative control, freshly prepared medium containing 10% fetal calf serum (FCS) was also examined, and no significant crossreaction was observed. (**D**) Biological effect of mouse IGF-I secreted by MS-5 cells on human hematopoietic cells was examined using NALM-16 cells that express IGF-IR. Cells at logarithmic growth were stimulated for 5 minutes with either freshly prepared culture medium containing 10% FCS, MS-5 culture supernatant, or recombinant mouse IGF-I (final concentration at 50 ng/mL) and examined by immunoblotting using antiphosphospecific human IGF-IR Ab that only recognize the activated form of IGF-IR. As a control, anti-entire IGF-IR Ab was also used.

human hematopoietic cells. Therefore, the data suggest a possibility that MS-5 cells secrete excess amounts of IGF-I and thus exogenous addition of recombinant IGF-I revealed no effect on pro–B-cell development.

Indeed, when anti-mouse IGF-I Ab, which neutralizes the effect of IGF-I, was added to the culture, development of $CD19^+$ B cells was significantly reduced (Fig. 3A and B). As shown in Figure 3B, the initial addition of 5 μg/mL polyclonal goat anti-mouse IGF-I Ab was sufficient to induce a significant reduction in pro–B-cell development. When hamster anti-mouse IGF-I mAb was used, however, additional Abs were required to produce a remarkable reduction in subsequent pro–B-cell production (Fig. 3A). In both cases, anti-mouse IGF-I Abs not only reduced the total cell number of cultured $CD34^+$ BM cells, but also remarkably diminished the percentage of $CD19^+$ B cells out of the total number of cells in the culture. Therefore, reduction in $CD19^+$ B cells is not merely the result of an overall cell reduction. Moreover, anti-mouse IGF-I Ab-induced reduction in $CD19^+$ B-cell development was cancelled by the addition of recombinant human IGF-I (Fig. 3D). The data suggests that IGF-I significantly participates in pro–B-cell development. Evidence that anti-human IGF-IR Ab and IGF-IR kinase inhibitor, both of which can block the effect of IGF-I, reduce pro–B-cell development, further supports this notion (Fig. 3B and C).

Of note, RT-PCR analysis also showed a time-dependent expression of IGF-I in a total cell fraction, but not sorted $CD19^+$ cell fraction, of the cultured human BM $CD34^+$ cells during the culture period (Fig. 2A). Beside $CD19^+$ cell fraction, $CD33^+$ myelomonocytic cells were present in the culture (data not shown). Although $CD33^+$ cell population was decreasing with the culture time, they matured with time. Thus, time-dependent expression of IGF-I is most likely due to this cell fraction.

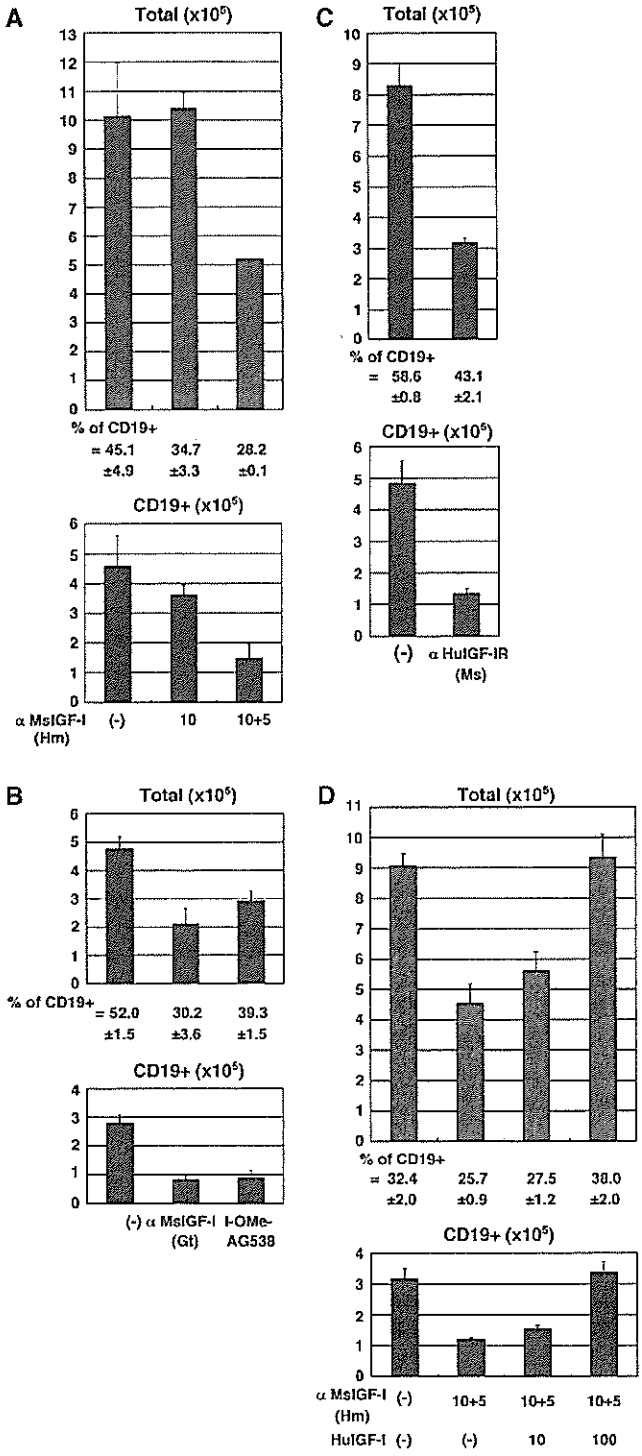

Effect of recombinant human IGFBPs on human pro–B-cell development

To assess the effect of IGFBPs on human pro–B-cell development, we challenged the present culture system with recombinant human IGFBPs. As shown in Figure 4A, of the six IGFBP members, only IGFBP-3 produced a subsequent reduction in the number of pro-B cells; the other IGFBPs did not affect human pro–B-cell development. As shown in Figure 4B, the inhibitory effect of IGFBP-3 on pro–B-cell differentiation was dose-dependent. Furthermore, IGFBP-3–mediated inhibition of $CD19^+$ cell development was cancelled by the addition of recombinant human IGF-I (Fig. 4C).

Because none of the IGFBPs other than IGFBP-3 affected pro–B-cell development from $CD34^+$ BM cells cocultured with MS-5, we tested a synergistic effect of two or more IGFBPs; no significant synergism was observed and other IGFBPs failed to enhance the effect of IGFBP3 (data not shown). Therefore, we next examined the effect of neutralization of the IGFBP function using specific Abs.

First we tested expression of IGFBPs in MS-5 cells. As shown in Figure 5A and B, RT-PCR experiments revealed that MS-5 transcribe mRNA of IGFBP-4, 5, and 6, but not 1, 2, and 3, while immunoblotting experiments using commercially available Abs detected only IGFBP-6 protein expression. Coincident with the results of immunoblotting, anti-IGFBP-2, 3, and 5 Abs did not affect MS-5–induced pro–B-cell development from $CD34^+$ BM cells (Fig. 5C). Interestingly, however, when anti-mouse IGFBP-6 Ab was added to the culture system, pro–B-cell development was significantly reduced (Fig. 5C). In addition, as shown in Figure 5D, the anti-mouse IGFBP-6 Ab–induced inhibition of pro–B-cell development was completely canceled by the addition of human IGFBP-6. In light of this data, we concluded that the IGFBP-6 produced by the MS-5 cells is essential for pro–B-cell development from $CD34^+$ BM cells.

Figure 3. Effect of insulin growth factor-I (IGF-I) inhibition on human pro–B-cell development. Human bone marrow (BM) $CD34^+$ cells were cocultured with MS-5 for 4 weeks in the presence or absence of hamster anti-mouse IGF-I monoclonal antibody (mAb) [(**A**) α MsIGF-I (Hm), either initial administration of 10 μg/mL alone (10) or a combination of an initial administration of 10 μg/mL and an additional administration of 5 μg/mL after 2 weeks of culture (10 + 5)], goat polyclonal anti-mouse IGF-I Ab [(**B**) α MsIGF-I (Gt), 5 μg/ml)], IGF-IR kinase inhibitor I-OMe-AG538 [(**B**) 5 μM], mouse anti-human IGF-IR mAb [(**C**) α HuIGF-IR (Ms), 5 μg/mL], and a combination of α MsIGF-1 (Hm) and human IGF-I (HuIGF-1, 10, and 100 ng/mL) (**D**). Subsequent $CD19^+$ cell number was estimated using flow cytometry and is shown. Total cell number of cultured $CD34^+$ cells and the percentage of $CD19^+$ cells are also presented.

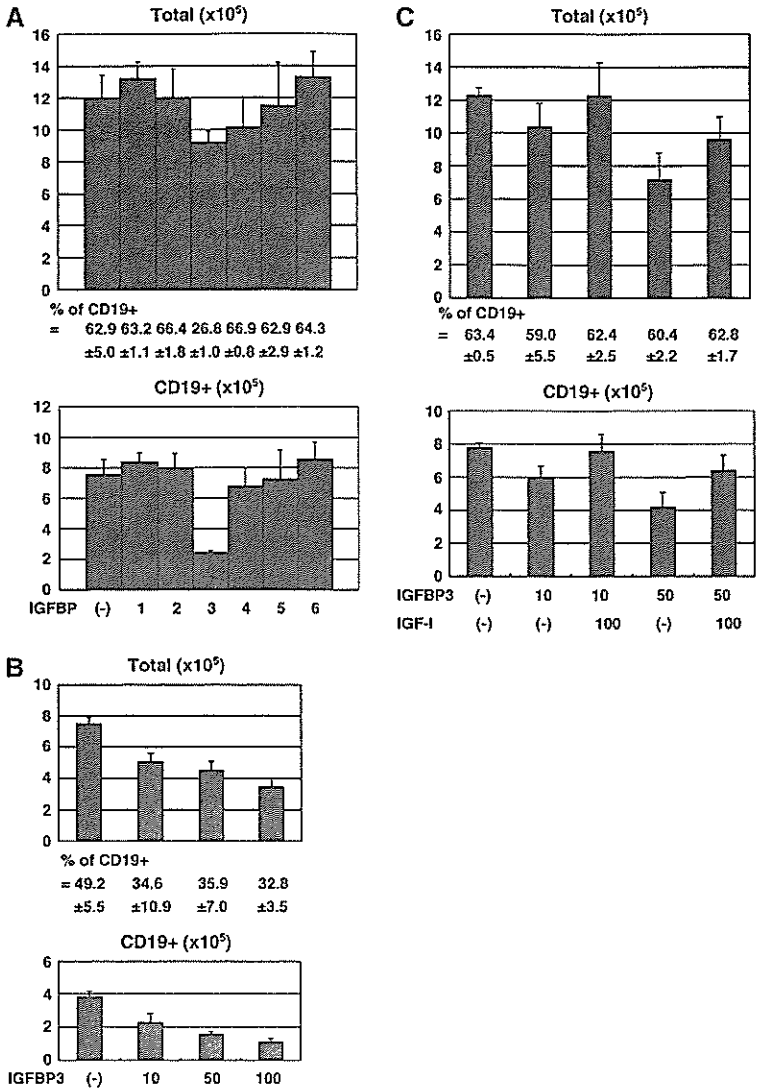

Figure 4. Effect of insulin-like growth factor (IGF)-binding proteins on human pro–B-cell development. (A) Human bone marrow (BM) $CD34^+$ cells were cocultured with MS-5 cells with or without 100 ng/mL each recombinant human IGF-binding proteins (IGFBP 1–6) for 4 weeks. The subsequent total cell number of cultured $CD34^+$ cells and the percentage and cell number of $CD19^+$ cells are shown. (B) Human BM $CD34^+$ cells were cocultured with MS-5 cells with or without different doses (ng/mL) of recombinant human IGFBP-3, as indicated, for 4 weeks and examined using the protocol described in (A). (C) Human BM $CD34^+$ cells were cocultured with MS-5 cells with or without indicated combinations of recombinant human IGFBP-3 (ng/mL) and human IGF-I (ng/mL) and examined using the protocol described in (A).

Discussion

In the present study, when BM $CD34^+$ cells were cultured in the presence of the murine stromal cell line MS-5, pro-B cells, but not pre-B cells, were efficiently induced. MS-5 is well known to be capable of supporting B-cell development [14–17]. However, several different groups have reported this cell line to have distinct effects on induction of B cells. Coincident with our observation, Berardi et al. [14] showed that when human HPSCs derived from umbilical CB were cultured in the presence of MS-5, $CD10^+$, $CD19^+$, and cytoplasmic μ^- pro-B cells were generated [14]. In contrast, Nishihara et al. [15] and Hirose et al. [16] reported the induction of pre-B cells from CB $CD34^+$ cells after coculturing with MS-5 in the presence of exogenous granulocyte colony-stimulating factor (G-CSF) and stem cell factor (SCF) [14–16]. Moreover, Ohkawara et al. [17] reported that surface IgM^+ mature B cells could be produced from CB $CD34^+$ cells using the same culture condition. We tested the effect of the exogenous addition of G-CSF and SCF in our culture system, but failed to observe any signs of pre–B-cell differentiation (data not shown). Although a precise reason for such a difference is unavailable, it may be possible that different stocks of MS-5 exhibit distinct effects on B-cell differentiation. A comparison of the distinct effects of different MS-5 stocks on B-cell differentiation may provide useful and interesting information.

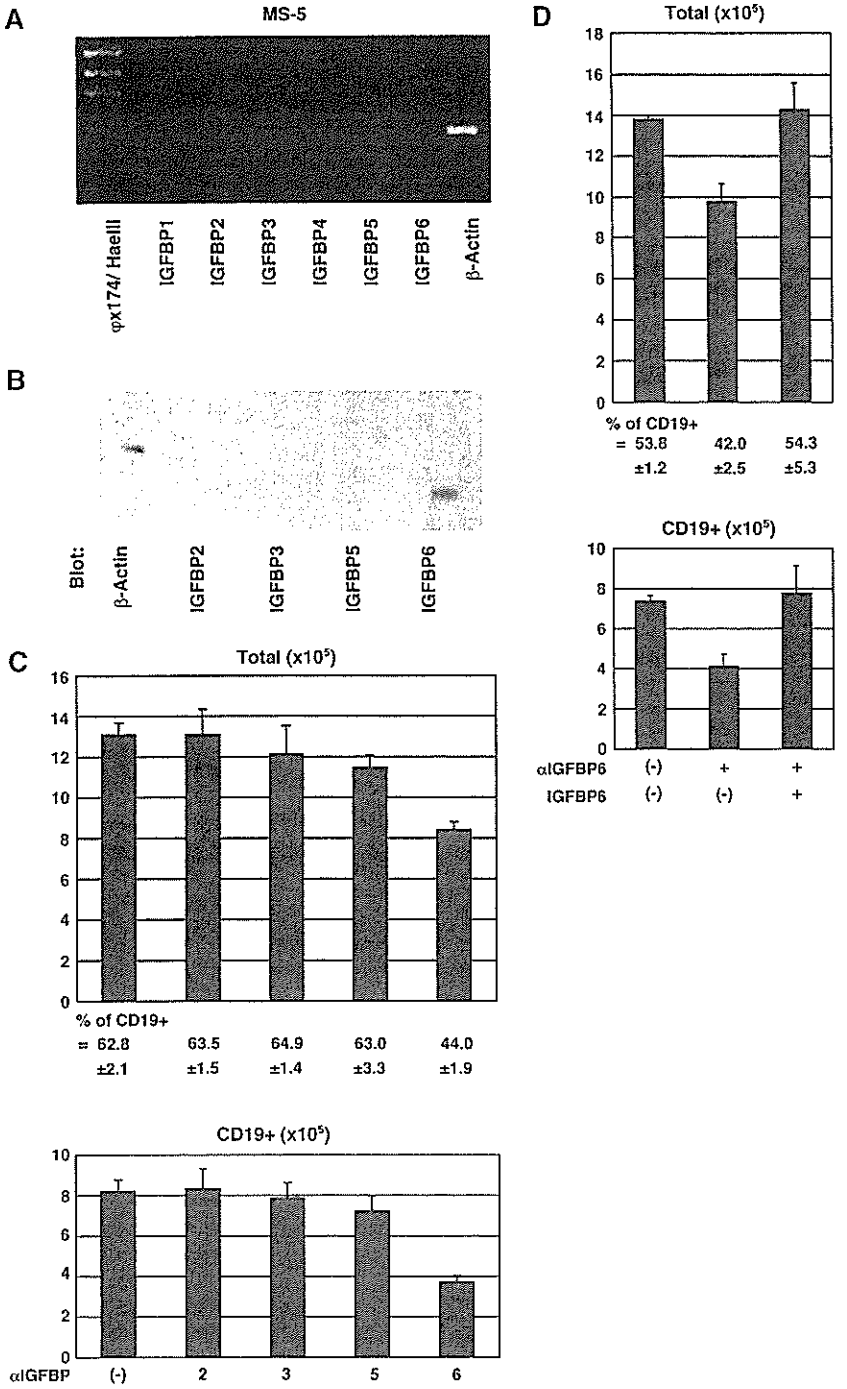

Figure 5. Effect of antibodies against insulin-like growth factor (IGF)-binding proteins on human pro–B-cell development. (**A**) Gene expression of mouse IGF-binding proteins (IGFBP) 1–6 on MS-5 cells was examined using reverse transcriptase polymerase chain reaction. As an internal control, expression of mouse β-actin was also examined. The φχ174/*Hae*III molecular weight marker was presented in the left side. (**B**) Immunoblot analysis with goat anti-mouse IGFBP-2, 3 5, and IGFBP-6 antibodies (αIGFBP2-6, respectively) on MS-5 cell lysates was performed. (**C**) Human bone marrow (BM) $CD34^+$ cells were cocultured with MS-5 cells for 4 weeks with or without 10 μg/mL each goat antibodies against mouse IGF-binding proteins (αIGFBP), as indicated. Subsequent cell number of $CD19^+$ cells was examined using flow cytometry and is shown. Total cell number of cultured $CD34^+$ cells and percentage of $CD19^+$ cells are also presented. (**D**) Human BM $CD34^+$ cells were cocultured with MS-5 cells for 4 weeks with or without the indicated combination of αIGFBP6 (5 μg/mL) and recombinant human IGFBP-6 (100 ng/mL). Subsequent total cell number of cultured $CD34^+$ cells and percentage and cell number of $CD19^+$ cells was examined using the protocol described in (C).

Table 1

Name of gene	Primer sequence forward reverse	Product size (bp)
human IGF-I	5′-ACAGGTATCGTGGATGAGTG-3′ 5′-GTAACTCGTGCAGAGCAAAG-3′	263
human IGF-IR	5′-ATGTGCTGGCAGTATAACCC-3′ 5′-ACAGCCTTGGATGAACGATG-3′	929
mouse IGF-I	5′-ATGCTCTTCAGTTCGTGTGT-3′ 5′-CTTCTCCTTTGCAGCTTCGT-3′	271
mouse IGFBP-1	5′-AGATTAGCTGCAGCCCAAC -3′ 5′-TGTTCTAGGCAGCATCACTCT-3′	535
mouse IGFBP-2	5′-ATCCCCAACTGTGACAAGCA-3′ 5′-CCTCTCTAACAGAAGCAAGGGA-3′	407
mouse IGFBP-3	5′-TCCAAGTTCCATCCACTCCA-3′ 5′-GAGGCAATGTACGTCGTCTT-3′	372
mouse IGFBP-4	5′-AATTAGAGATCGGAGCAAGA-3′ 5′-TGGGAATTCCTATTGCTACA-3′	598
mouse IGFBP-5	5′-ATGAGACAGGAATCCGAACA-3′ 5′-TCAACGTTACTGCTGTCGAA-3′	269
mouse IGFBP-6	5′-TGCTAATGCTGTTGTTCGCT-3′ 5′-TGAGTGCTTCCTTGACCATC-3′	652
human GAPDH	5′-CCACCCATGGCAAATTCCATGGCA-3′ 5′-TCTAGACGGCAGGTCAGGTCCACC-3′	598
mouse Actin	5′-TGACGGGGTCACCCACACTGTGCCCATCTA-3′ 5′-CTAGAAGCATTTGCGGTGGACGATGGAGGG-3′	661

It was previously reported that earlier stages of B-cell development depend on contact with the stromal cells [15,17]. Consistently, culture supernatant of MS-5 cells failed to support pro–B-cell development from $CD34^+$ BM cells (data not shown), suggesting that cell-to-cell interaction between $CD34^+$ BM cells and MS-5 cells is essential for pro–B-cell development in our culture system. In contrast, however, we detected pro-B cells not only in adherent cell fraction, but also in floating cell fraction, while pro-B cells were more enriched in adherent cell fraction. Although contact with stromal cells should be necessary for pro-B cell development from $CD34^+$ cells, it may not always be necessary for further differentiation and/or proliferation of pro-B cells. Therefore, a portion of pro-B cells will dissociate from stromal cells and move to floating cell fraction.

As demonstrated in the present study, the MS-5 cells produced IGF-I, and elimination of IGF-I function resulted in the failure of pro–B-cell development. Previous reports have revealed that IGF-I is essential for differentiation of pro-B to pre-B cell [6,18] and expansion of B-cell population [7,8]. Therefore, our data extends previous observations and indicates that IGF-I likely plays an important role in induction of pro-B cells from HPSCs.

As we presented in Figure 2A, IGF-I is possibly secreted by a non–B-cell fraction of the cultured $CD34^+$ cells. IGF-I may also be present in the supplemented FCS. Therefore, in addition to the IGF-I secreted by MS-5 cells, IGF-I produced by a non–B-cell fraction of the cultured $CD34^+$ cells as well as that provided by supplemented FCS can also affect to pro–B-cell development. However, as we presented in Figure 2D, the biological assay has indicated that the contribution of IGF-I that may be present in the supplemented FCS can be excluded. Furthermore, because the Abs used to neutralize IGF-I activity in this study have higher specificity for mouse IGF-I than human IGF-I, it is most likely that the majority of IGF-I–mediated effects in our culture system are due to mouse IGF-I secreted by MS-5 cells.

Because IGF-I is thought to play an integrating role in hematopoiesis, it seems reasonable to consider that IGFBPs may also contribute to regulation of hematopoiesis. Evidence that IGFBPs are produced by stromal cells in the BM, yolk sac, and liver, where hematopoiesis occurs [19,20], strongly supports this notion. Indeed, a recent report by Liu et al. [21] suggested that IGFBP-3 may block differentiation of HPSCs and be capable of promoting proliferation of primitive $CD34^+CD38^-$ hematopoietic cells, contributing to expansion of the HPSC pool [21]. In this study, we further demonstrated that addition of exogenous IGFBP-3 inhibited the effect of IGF-I on pro–B-cell induction from $CD34^+$ BM cells. Although MS-5 cells do not express IGFBP-3, it has been reported that BM stromal cells produce IGFBP-3 upon stimulation with several factors, such as vitamin D3 and transforming growth factor (TGF)-β1 [22,23]. Therefore, it is conceivable that IGFBP-3 could be secreted by BM stromal cells and involved in the regulation of early hematopoiesis, including B-cell development, depending on conditions in the hematopoietic microenvironment.

As demonstrated in the present article, while all six members of the IGFBP family possess the ability to bind with IGF, only IGFBP-3 inhibited the effect of IGF-I on

pro–B-cell development. Because all other IGFBPs failed to exert synergism with the IGFBP-3 in an inhibitory effect on pro–B-cell development in our experiment (data not shown), IGFBPs may compete with each other for binding with IGF-I, and IGFBP-3 should have the highest binding affinity. Furthermore, our data indicated that IGFBP-6 is required for pro–B-cell development, and neutralization of IGFBP-6 resulted in a marked reduction in the subsequent pro–B-cell number. Therefore, it is suggested that each IGFBP can have a distinct effect on the IGF action in regulation of hematopoiesis.

Interestingly, recent reports have indicated that IGFBPs have an intrinsic ability to affect cells directly [24–29]. For example, IGFBP-2 has been shown to be mitogenic in uterine endometrial and osteosarcoma cells in the absence of IGFs [30]. IGFBP-3 has been reported to induce a reduction in cell growth, DNA synthesis inhibition, and apoptosis in specific cells in an IGF-independent manner [31–34]. Furthermore, IGFBPs have been reported to have specific cell-surface receptors; IGFBP-2 and IGFBP-3 directly bind to target cells through $\alpha5\beta1$ integrin and TGF-β type-V receptors, respectively, thereby inducing intracellular signals [35,36]. Therefore, IGFBPs might not only inhibit the effects of IGF-I during hematopoiesis, but also have intrinsic and direct bioactivities that directly affect hematopoietic cells independently of IGF-I function.

In conclusion, IGF-I and IGFBPs appear to play important roles in early B-lymphopoiesis. Although details of their molecular functions remain uncertain, IGFBPs can possibly affect hematopoietic cells in both IGF-dependent and IGF-independent manners. The present observations should contribute to a better understanding of the functional roles of IGF-I and IGFBPs in regulation of B-lymphopoiesis.

Acknowledgments

We thank S. Yamauchi for her excellent secretarial work. We also thank Dr. A. Manabe, Dr. K. J. Mori, and Dr. Y. Matsuo for gifting murine BM stromal cell line, MS-5, and human leukemia cell line HPB-NULL. This work is supported in part by MEXT. KAKENHI 16017321, JSPS. KAKENHI 17591131, the Budget for Nuclear Research of the Ministry of Education, Culture, Sports, Science and Technology, based on the screening and counseling by the Atomic Energy Commission, grant from the Japan Health Sciences Foundation for Research on Health Sciences Focusing on Drug Innovation, and a Grant for Child Health and Development from the Ministry of Health, Labour and Welfare. T. Taguchi is an Awardee of Research Resident Fellowship from the Foundation for Promotion of Cancer Research (Japan) for the 3rd Term Comprehensive 10-Years-Strategy for Cancer Control.

References

1. Clark R. The somatogenic hormones and insulin-like growth factor-1: stimulators of lymphopoiesis and immune function. Endocr Rev. 1997; 18:157–179.
2. Baxter RC. Insulin-like growth factor (IGF)-binding proteins: interactions with IGFs and intrinsic bioactivities. Am J Physiol. 2000;278: E967–E976.
3. Rajaram S, Baylink DJ, Mohan S. Insulin-like growth factor-binding proteins in serum and other biological fluids: regulation and functions. Endocr Rev. 1997;18:801–831.
4. Firth SM, Baxter RC. Cellular actions of the insulin-like growth factor binding proteins. Endocr Rev. 2002;23:824–854.
5. Kurtz A, Matter R, Eckardt KU, Zapf J. Erythropoiesis, serum erythropoietin, and serum IGF-I in rats during accelerated growth. Acta Endocrinol (Copenh). 1990;122:323–328.
6. Landreth KS, Narayanan R, Dorshkind K. Insulin-like growth factor-I regulates pro-B cell differentiation. Blood. 1992;80:1207–1212.
7. Gibson LF, Piktel D, Landreth KS. Insulin-like growth factor-1 potentiates expansion of interleukin-7-dependent pro-B cells. Blood. 1993; 82:3005–3011.
8. Jardieu P, Clark R, Mortensen D, Dorshkind K. In vivo administration of insulin-like growth factor-I stimulates primary B lymphopoiesis and enhances lymphocyte recovery after bone marrow transplantation. J Immunol. 1994;152:4320–4327.
9. Melchers F, Karasuyama H, Haasner D, et al. The surrogate light chain in B-cell development. Immunol Today. 1993;14:60–68.
10. Kiyokawa N, Kokai Y, Ishimoto K, Fujita H, Fujimoto J, Hata J. Characterization of the common acute lymphoblastic leukemia antigen (CD10) as an activation molecule on mature human B cells. Clin Exp Immunol. 1990;79:322–327.
11. Takenouchi H, Kiyokawa N, Taguchi T, et al. Shiga toxin binding to globotriaosyl ceramide induces intracellular signals that mediate cytoskeleton remodeling in human renal carcinoma-derived cells. J Cell Sci. 2004;117:3911–3922.
12. Saito M, Kiyokawa N, Taguchi T, et al. Granulocyte colony-stimulating factor directly affects human monocytes and modulates cytokine secretion. Exp Hematol. 2002;30:1115–1123.
13. Kiyokawa N, Lee EK, Karunagaran D, Lin S-Y, Hung M-C. Mitosis-specific negative regulation of epidermal growth factor receptor, triggered by a decrease in ligand binding and dimerization, can be overcome by overexpression of receptor. J Biol Chem. 1997;272: 18656–18665.
14. Berardi AC, Meffre E, Pflumio F, et al. Individual CD34+ CD38lowCD19-CD10- progenitor cells from human cord blood generate B lymphocytes and granulocytes. Blood. 1997;89:3554–3564.
15. Nishihara M, Wada Y, Ogami K, et al. A combination of stem cell factor and granulocyte colony-stimulating factor enhances the growth of human progenitor B cells supported by murine stromal cell line MS-5. Eur J Immunol. 1998;28:855–864.
16. Hirose Y, Kiyoi H, Itoh K, Kato K, Saito H, Naoe T. B-cell precursors differentiated from cord blood CD34+ cells are more immature than those derived from granulocyte colony-stimulating factor-mobilized peripheral blood CD34+ cells. Immunology. 2001;104:410–417.
17. Ohkawara JI, Ikebuchi K, Fujihara M, et al. Culture system for extensive production of CD19+IgM+ cells by human cord blood CD34+ progenitors. Leukemia. 1998;12:764–771.
18. Funk PE, Kincade PW, Witte PL. Native associations of early hematopoietic stem cells and stromal cells isolated in bone marrow cell aggregates. Blood. 1994;83:361–369.
19. Clawson TF, Lee WH, Yoder MC. Differential expression of insulin-like growth factor binding proteins in murine hematopoietic stromal cell lines. Mol Cell Endocrinol. 1996;120:59–66.
20. Abboud SL, Bethel CR, Aron DC. Secretion of insulinlike growth factor I and insulinlike growth factor-binding proteins by murine bone marrow stromal cells. J Clin Invest. 1991;88:470–475.
21. Liu LQ, Sposato M, Liu HY, et al. Functional cloning of IGFBP-3 from human microvascular endothelial cells reveals its novel role in promoting proliferation of primitive CD34+CD38- hematopoietic cells in vitro. Oncol Res. 2003;13:359–371.

22. Kveiborg M, Flyvbjerg A, Eriksen EF, Kassem M. 1,25-Dihydroxyvitamin D3 stimulates the production of insulin-like growth factor-binding proteins-2, -3 and -4 inhuman bone marrow stromal cells. Eur J Endocrinol. 2001;144:549–557.
23. Kveiborg M, Flyvbjerg A, Eriksen EF, Kassem M. Transforming growth factor-beta1 stimulates the production of insulin-like growth factor-I and insulin-like growth factor-binding protein-3 in human bone marrow stromal osteoblast progenitors. J Endocrinol. 2001; 169:549–561.
24. Valentinis B, Bhala A, DeAngelis T, Baserga R, Cohen P. The human insulin-like growth factor (IGF) binding protein-3 inhibits the growth of fibroblasts with a targeted disruption of the IGF-I receptor gene. Mol Endocrinol. 1995;9:361–367.
25. Oh Y, Muller HL, Lamson G, Rosenfeld RG. Insulin-like growth factor (IGF)-independent action of IGF-binding protein-3 in Hs578T human breast cancer cells. Cell surface binding and growth inhibition. J Biol Chem. 1993;268:14964–14971.
26. Oh Y, Muller HL, Pham H, Rosenfeld RG. Demonstration of receptors for insulin-like growth factor binding protein-3 on Hs578T human breast cancer cells. J Biol Chem. 1993;268:26045–26048.
27. Rajah R, Valentinis B, Cohen P. Insulin-like growth factor (IGF)-binding protein-3 induces apoptosis and mediates the effects of transforming growth factor-beta1 on programmed cell death through a p53- and IGF-independent mechanism. J Biol Chem. 1997;272: 12181–12188.
28. Conover CA, Bale LK, Durham SK, Powell DR. Insulin-like growth factor (IGF) binding protein-3 potentiation of IGF action is mediated through the phosphatidylinositol-3-kinase pathway and is associated with alteration in protein kinase B/AKT sensitivity. Endocrinology. 2000;141:3098–3103.
29. Rajah R, Lee KW, Cohen P. Insulin-like growth factor binding protein-3 mediates tumor necrosis factor-alpha-induced apoptosis: role of Bcl-2 phosphorylation. Cell Growth Differ. 2002;13:163–171.
30. Slootweg MC, Ohlsson C, Salles JP, de Vries CP, Netelenbos JC. Insulin-like growth factor binding proteins-2 and -3 stimulate growth hormone receptor binding and mitogenesis in rat osteosarcoma cells. Endocrinology. 1995;136:4210–4217.
31. Villaudy J, Delbe J, Blat C, Desauty G, Golde A, Harel L. An IGF binding protein is an inhibitor of FGF stimulation. J Cell Physiol. 1991;149:492–496.
32. Imbenotte J, Liu L, Desauty G, Harel L. Stimulation by TGF beta of chick embryo fibroblasts—inhibition by an IGFBP-3. Exp Cell Res. 1992;199:229–233.
33. Cohen P, Lamson G, Okajima T, Rosenfeld RG. Transfection of the human IGFBP-3 gene into Balb/c fibroblasts: a model for the cellular functions of IGFBPs. Growth Regul. 1993;3:23–26.
34. Bernard L, Babajko S, Binoux M, Ricort JM. The amino-terminal region of insulin-like growth factor binding protein-3, (1-95)IGFBP-3, induces apoptosis of MCF-7 breast carcinoma cells. Biochem Biophys Res Commun. 2002;293:55–60.
35. Schutt BS, Langkamp M, Ranke MB, Elmlinger MW. Intracellular signalling of insulin-like growth factor binding protein-2 [abstract]. Growth Horm IGF Res. 2000;0. A29.
36. Leal SM, Liu Q, Huang SS, Huang JS. The type V transforming growth factor beta receptor is the putative insulin-like growth factor-binding protein 3 receptor. J Biol Chem. 1997;272:20572–20576.

Pathology International 2006; **56**: 543–548 doi:10.1111/j.1440-1827.2006.02003.x

Case Report

Desmoplastic small cell tumor of soft tissue: Molecular variant of *EWS-WT1* chimeric fusion

Minoru Hamazaki,[1] Hajime Okita,[2] Jun-ichi Hata,[3] Shin-ichi Shimizu,[4] Hiroshi Kobayashi,[4] Katsuhiko Aoki[5] and Taemi Nara[6]

Departments of [1]Pathology, [5]Radiology and [6]Oncology, Shizuoka Children's Hospital, Shizuoka, [2]Department of Developmental Biology, National Research Institute for Child Health and Development, [3]National Center for Child Health and Development, Tokyo and [4]Department of Pathology, Seirei Hamamatsu General Hospital, Hamamatsu, Japan

A 7-year-old girl was hospitalized because of a tumorous mass in her left periorbital region. The tumor was removed by local excision. The soft-part tumor recurred in the parotid gland region 4 months later, and a second recurrence was noted on the left side of the neck 3 years and 3 months thereafter. The patient had not received chemotherapy or local irradiation. Histological and immunohistochemical examinations of the recurrent masses revealed morphological characteristics of small cell proliferation with desmoplastic stroma that were similar to those of the initial tumor. The cellular components showed immunoreactivity for desmin, cytokeratin, vimentin, and epithelial membrane antigen in part, but the cells were negative for myogenin, CD99, and neuron-specific enolase. These findings suggested a diagnosis of desmoplastic small cell tumor, despite its extra-abdominal location. The histological diagnosis was confirmed by reverse transcriptase polymerase chain reaction, which demonstrated an *EWS-WT1* chimeric fusion gene. An in-frame fusion of *EWS* exon 9 and *WT1* exon 8 was subsequently identified by cloning and sequencing. The chimeric fusion gene might be related to the tissue-specific phenotype of desmoplastic small cell tumors, although further investigation of this speculation is necessary.

Key words: desmoplastic small cell tumor, *EWS-WT1* fusion transcript, extra-abdominal

Desmoplastic small cell tumor (DSCT) occurs usually in the intra-abdominal region of children or adolescents and consists of proliferating small cells with a desmoplastic stroma. DSCT is also characterized by the presence of an *EWS-WT1* chimeric fusion transcript, typically confirmed by reverse transcriptase–polymerase chain reaction (RT-PCR). Tumors with similar histological appearances have been reported in other soft tissues,[1] but such tumors are extremely rare. Here, we describe a patient with a desmoplastic small cell tumor that developed primarily in the orbital soft tissue.

CLINICAL SUMMARY

A 7-year-old girl complained of an insidious swelling in the soft tissue of her left upper eyelid. On hospitalization, a reconstructed CT image revealed a partially calcified, low-density mass in the upper lateral aspect of the left orbital region (Fig. 1). The mass was excised surgically. The patient was not treated with systemic chemotherapy or local irradiation.

Four months after the initial surgery, a local recurrence was detected in the left periorbital region. A CT image revealed an irregular mass, measuring 26 × 20 mm in greatest diameter, with central low-density and calcified foci; the mass was located near the upper aspect of the left parotid gland (Fig. 1). Systemic gallium citrate scintigraphy demonstrated an abnormally localized accumulation at the mass lesion, but no distant metastases were noted. The local tumor was completely re-excised surgically, and the patient was carefully followed thereafter. Chemotherapy or irradiation was not performed.

Three years and 3 months later, at the age of 11 years, the patient was again hospitalized because of a second recurrence in her left lower neck region. CT showed a tumorous lesion located between the left lower margin of the parotid gland and the piriform fossa. The main cervical recurrent tumor and nodal metastases were removed. The tumorous tissue weighed 38.9 g in total. The patient has been followed for 8 months and has shown no signs of local recurrence,

Correspondence: Minoru Hamazaki, MD, Department of Pathology, Shizuoka Children's Hospital, 860 Urushiyama, Aoi-ku, Shizuoka 420-8660, Japan. Email: mhamasan@sch.pref.shizuoka.jp

Received 13 March 2006. Accepted for publication 1 May 2006.

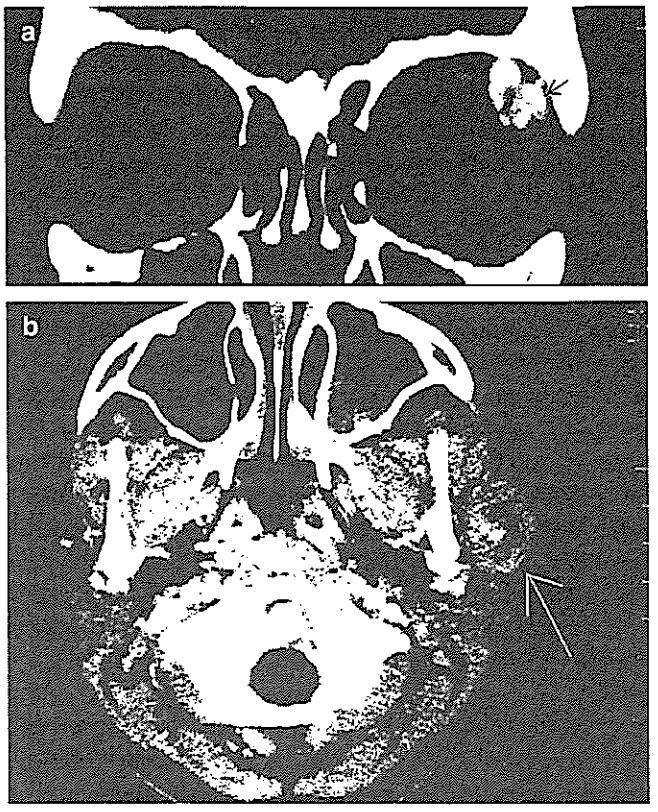

Figure 1 Radiological appearance. (a) The initial tumor mass (arrow) is visible in the left upper lateral aspect of the orbital region as a partially calcified, low-density mass on a CT image. (b) CT of the first recurrence showing an irregular mass (arrow) with a central low-density area near the upper aspect of the left parotid gland.

although the possibility of future recurrence cannot be ruled out.

PATHOLOGICAL FINDINGS

A conventional morphological examination was performed using formalin-fixed paraffin sections stained with HE. Histological examination of the primary tumor suggested an epithelial neoplasm, like a lacrimal gland carcinoma or an adenoid cystic carcinoma, or a rhabdomyosarcoma or metastasis of an abdominal tumor. The first recurrent tumor was characterized by conspicuously atypical small cell proliferation, forming solid cellular nodules or trabecular, basaloid epithelial lesions, and was accompanied by prominent interstitial fibrous intervention (Fig. 2). The tumorous tissue was intermingled with the ducts of the parotid gland, and the tumor itself was located adjacent to the serous acini of the parotid gland. The second recurrent main tumor exhibited diffuse cellular proliferation but did not have a desmoplastic stroma. The nodal metastases in the lower portion of the left neck, however, exhibited a distinct desmoplastic morphology similar to that of the first recurrent tumor. These histological findings were consistent with a desmoplastic small cell tumor of soft tissue with divergent differentiation, and were almost identical to those of the initial orbital tumor.

Immunohistochemical study

The immunohistochemical investigation was performed using formalin-fixed, paraffin-embedded tissues and the streptoavidin–biotin peroxidase indirect method. Primary antibodies were prepared against the following antigens: desmin (clone DE-R-11, diluted 1:50; DakoCytomation, Glostrup, Denmark), cytokeratin (AE1/AE3, diluted 1:50, proteinase K-treated; DakoCytomation), vimentin (Vim3B4, diluted 1:50, microwave-treated; DakoCytomation), epithelial membrane antigen (EMA; E29, diluted 1:50; DakoCytomation), myogenin (F5D, diluted 1:50, microwave-treated; DakoCytomation), WT1 (C-19, diluted 1:50, proteinase K-treated; Santa Cruz Biotechnology, Santa Cruz, CA, USA), CD99 (F5D, diluted 1:50; DakoCytomation), sarcomeric actin (α-Sr-1, diluted 1:40; DakoCytomation), CD45 (T29/33, diluted 1:50; DakoCytomation), glial fibrillary acidic protein (GFAP; 6F2, diluted 1:50, microwave-treated; DakoCytomation), neuron-specific enolase (NSE; BBS/NC/VI-H14, diluted 1:50; DakoCytomation), S-100 protein (rabbit polyclonal, diluted 1:400; DakoCytomation), Ki-67 antigen (MIB-1, diluted 1:50, microwave-treated; DakoCytomation), and P53 (PAb240, diluted 1:50, microwave-treated; DakoCytomation).

The solid areas of the first and second recurrent tumors were positive for vimentin, but the trabeculae were negative. In contrast, the trabecular or epithelioid components were positive for EMA, but the solid cellular area was negative. Distinct positive immunoreactivity for desmin and cytokeratin was expressed in the cytoplasm of the small tumor cells in both the solid cellular and trabecular architectures (Fig. 3). No evidence of myogenin, WT1, CD99, sarcomeric actin, CD45, GFAP, NSE, or S-100 protein positivity was seen. Ki-67 labeling index was 40–60% in the solid area of tumor and 10–20% at the trabeculae. P53 labeling index was <1–5%.

Electron microscopy

The electron microscopy specimens were prepared using conventional 2% glutaraldehyde and 1% osmium tetraoxide fixation followed by epoxy embedding. Ultrathin sections stained with uranyl acetate and lead citrate were then observed using a JEM 1010 transmission electron microscope (JEOL, Tokyo, Japan).

The tumor cells were characterized by prominent desmosome-type intercellular junctions with tonofilaments (Fig. 4). A small amount of intermediate fibrils without striated muscle

Figure 2 Histological findings. (a) Conspicuous proliferation of small atypical cells with increased mitotic figures is apparent. A salivary gland duct is visible at the right of the figure. (b) The tumor tissue is characterized by trabecular, epithelioid proliferation surrounded by a hyaline basal structure, with fibrous proliferation in the interstitium.

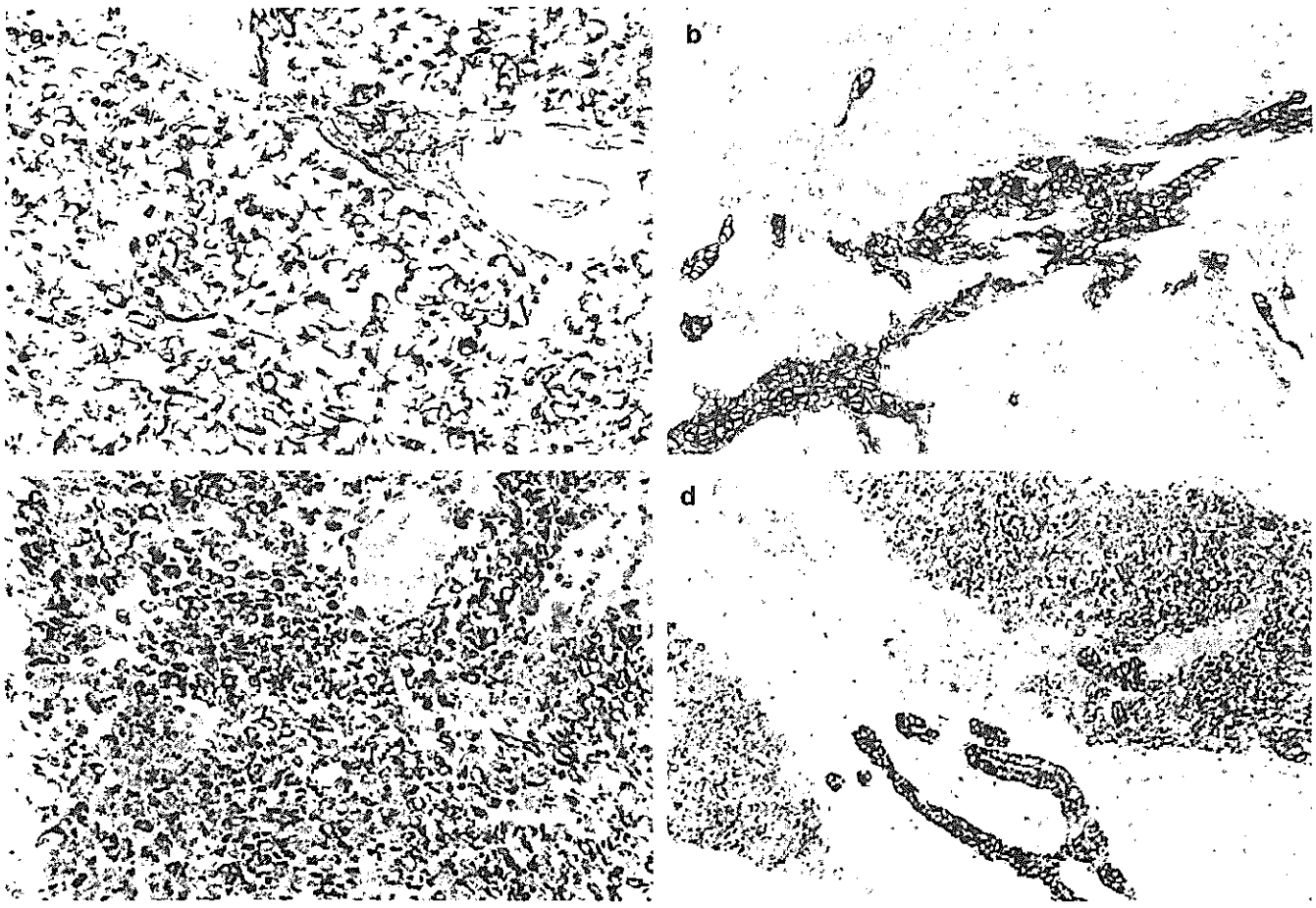

Figure 3 Immunohistochemical findings. (a) Vimentin is reactive in the cytoplasm of the tumor cells. (b) EMA is positive at the membrane of the tumor cells, especially in the trabecular region. Immunostaining was positive for (c) desmin and (d) cytokeratin in both solid and trabecular portions of the tumor.

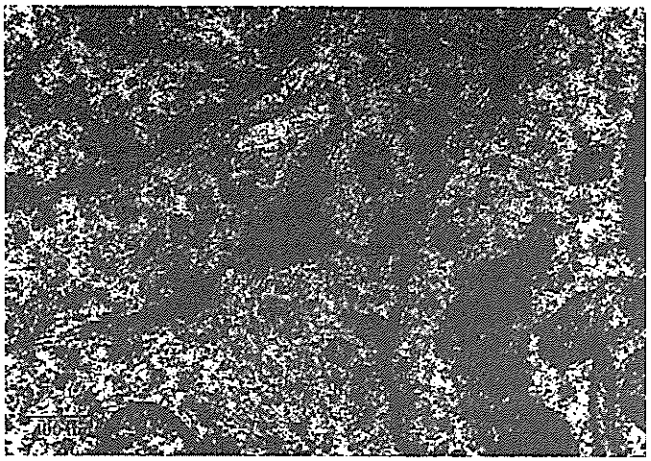

Figure 4 Electron microscopy. The tumor cells exhibit intercellular desmosomes with distinct tonofilaments.

differentiation were seen in the cytoplasm. No specific neurosecretory vesicle was found in the cytoplasm.

Gene analysis

Total RNA was extracted from frozen tumor tissue using an RNeasy Kit (Qiagen, Hilden, Germany) and was reverse transcribed to cDNA using a First-Strand cDNA synthesis Kit (Amersham, Piscataway, NJ, USA). PCR was performed using the following primers: EWS/WT1, ESBP1 (CGAC TAGTTATGATCAGAGCAGT)[2] and 10BA (TGCTGCCTGG GACACTGAAC); EWS-FLI1, 22.3 (TCCTACAGCCAAGCT CCAAGTC)[3] and 11.3 (ACTCCCCGTTGGTCCCCTCC); and EWS/ERG, ESBP1 and EU15 (CATGTACGGGAGGTCT GAGGGGT).[4] The amplified products were run on a 2% agarose gel. The products were then purified using MicroSpin S-400 Columns (Amersham) and cloned into pGEM-T vectors via the pGEM-T Vector System (Promega, Madison, WI, USA). Sequencing of the subcloned PCR products was performed using a DyEnamic ET Terminator Cycle Sequencing Kit (Amersham) with M13-40 and reverse primers.

The aforementioned histological diagnosis was also confirmed by RT-PCR of snap-frozen tumor tissues taken from the first recurrent tumor and the second recurrent masses, including both the solid cellular portion and the desmoplastic portion (Fig. 5). Each tissue specimen exhibited the same *EWS-WT1* chimeric fusion (data not shown). The chimeric transcript was finally confirmed by cloning and sequencing of the PCR product, resulting in the identification of an in-frame fusion of *EWS* exon 9 and *WT1* exon 8 (Fig. 6). Neither *EWS-FLI1* nor *EWS-ERG* chimeric transcripts associated with the Ewing family of tumors were detected (data not shown).

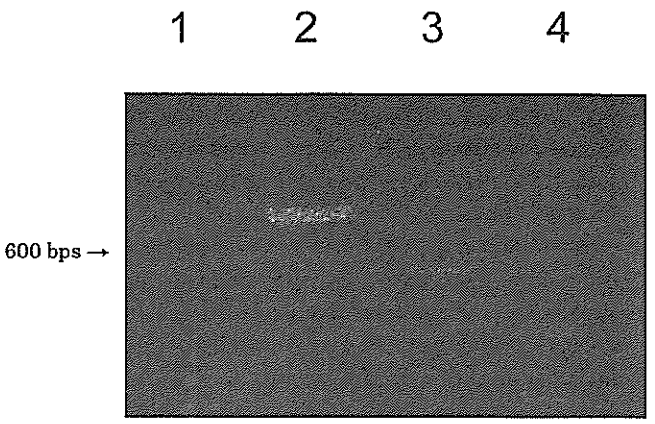

Figure 5 Molecular analysis. Reverse transcriptase–polymerase chain reaction of the first recurrent tumor tissue shows an in-frame fusion of *EWS* and *WT1* in lane 2, which contains a longer band than that of the positive desmoplastic small cell tumor (DSCT) control. A smaller product, corresponding to the fusion of *EWS* exon 7 to *WT1* exon 8, is also visible. Lane 1, 100 bp ladder marker; lane 2, present case; lane 3, positive DSCT control; lane 4, *NCR-NB3* negative control neuroblastoma cell.

	EWS exon 9	WT1 exon 8
Present case	cgaggtggcttcaataagcctggtg	gtgagaaaccataccagtgtgactt

Figure 6 Sequence of *EWS-WT1* junction. The fusion point of the longer product is shown. A vertical line indicates the nucleotide position of the junction.

DISCUSSION

Several epithelial neoplasms, many of which are malignant in adults, were initially considered in the differential diagnosis of the slow-growing tumor and repeated recurrences seen in the present case. Several kinds of malignant small cell tumors of soft tissues including rhabdomyosarcoma (especially alveolar type), extraskeletal Ewing sarcoma family of tumors (ESFT),[5] neuroblastoma metastases, and non-Hodgkin lymphoma (in addition to DSCT) must be ruled out in pediatric patients. The immunohistochemical reactivity of desmin or vimentin was not necessary to confirm a diagnosis of rhabdomyosarcoma because myogenin, which is a myogenic regulatory protein, was not reactive. The absence of CD99, CD45, NSE, S100, and GFAP reactivity enabled ESFT, non-Hodgkin lymphoma, and neuronal tumors to be ruled out. Electron microscopy revealed an epithelioid fine structure with distinct desmosomes, similar to the findings for a previously reported extra-abdominal DSCT.[6] No evidence of intracytoplasmic neurosecretory vesicles, often seen in neuroblastomas, or aggregates of thick myofilaments with electron-dense zones, indicating rhabdomyosarcoma, was found.

Another possibility in the differential diagnosis of small round cell tumors in children is DSCT. Recently, intra-

abdominal DSCT was recognized as a small cell tumor that usually occurs in the intra-abdominal region of children or young adults. DSCT is characterized by small cell proliferation, prominent stromal desmoplasia, and intra-abdominal serosal involvement. A distinct molecular property of this tumor is the presence of an in-frame fusion of the *EWS* gene and the *WT1* gene.[7–11]

Intra-abdominal DSCT has been described in the retroperitoneum, pancreatic region, gastric wall, and the pelvic, mesenteric, and omental regions.[7,9,12] Light microcopy has revealed a divergent differentiation pattern (small cell proliferation in an intermingled pattern) because the majority of cases exhibit a trabecular, basalioid, or glandular architecture associated with abundant interstitial fibrous proliferation, and, in some cases, solid cellular areas.[7] The small cells are typically positive for cytokeratin, EMA, vimentin, desmin, or NSE immunohistochemical staining.[7] Immunoreactivity for S100, Leu7, or LeuM1 has been observed in some cases.[6,13–20]

Cytogenetic investigation of intra-abdominal DSCT has revealed a consistent chromosomal translocation: t(11;22)(p13;q12). This translocation causes an in-frame fusion between the *EWS* gene and the *WT1* gene, producing a chimeric transcript. In most cases of intra-abdominal DSCT, the first seven exons of *EWS* are fused to the last three exons of *WT1*. *EWS-ERG* or *EWS-FLI1* fusion transcripts have also been described in some DSCT cases.[10–12,21]

The soft-tissue tumor in the present case was similarly characterized by divergent immunoreactivity pattern of EMA, cytokeratin, desmin, and vimentin in the solid and trabecular areas of the tumor. Electron microscopy showed the tumor cells to be arrayed with distinct desmosome-type intercellular junctions[6] and with intracytoplasmic intermediate fibrils in a few cells. These characteristics were morphologically and immunohistochemically consistent with a diagnosis of DSCT, despite the extra-abdominal location of the tumor. Molecular analysis of the first and second recurrent tumors showed the same in-frame fusion transcript, even though the tumor tissues had different morphological phenotypes.

Extra-abdominal DSCT is extremely rare, although ovarian or paratesticular involvement has been described.[13–15] DSCT of the soft tissue and bone of the hand, intracranial DSCT, and pleural cavity DSCT have also been reported.[16–19] To the best of our knowledge, no extra-abdominal DSCT confirmed by RT-PCR to exhibit an *EWS-WT1* chimeric fusion have been reported in Japanese studies. The morphological, immunohistochemical, ultrastructural, and molecular features of soft-tissue DSCT are similar to those of intra-abdominal DSCT. Gerald *et al.* reviewed and summarized 109 cases of DSCT, of which 103 were located in the abdominal cavity, four were in the thoracic region, one was in the cranial fossa, and one was in the hand.[20] Swanson *et al.* described 12 cases of polyphenotypic small cell tumors in children; two of these tumors arose from bone, six arose from soft tissue or the axial skeleton, two arose from the CNS, and two arose from the retroperitoneum.[1] All of the tumors exhibited primitive round cell features or neuroectodermal characteristics with or without myogenic, epithelial, or combined differentiation.

The present patient exhibited an uncommon form of the *EWS-WT1* fusion transcript: a fusion of *EWS* exon 9 and *WT1* exon 8, instead of the more common fusion of *EWS* exon 7 and *WT1* exon 8 seen in intra-abdominal DSCT.[8,22] Interestingly, two cases of DSCT of soft tissue and bone and one case of DSCT of the kidney exhibited the same type of fusion transcript.[6,19,23] This molecular aberration might be a variant of the in-frame *EWS-WT1* fusion transcript, because the *EWS-WT1* fusion gene has been reported to exhibit molecular heterogeneity, such as the fusion of *EWS* exon 10 and *WT1* exon 8[24] or the fusion of *EWS* exon 7 and *WT1* exon 9.[12] In contrast, intra-abdominal DSCT with a fusion of *EWS* exon 9 and *WT1* exon 8 has not been previously described. Furthermore, in spite of the cytological heterogeneity of the tumor phenotypes in the present case, the same in-frame *EWS-WT1* fusion was noted in the solid area and the desmoplastic epithelioid region. The genetic findings in the present case suggest that fusion gene heterogeneity may be related to the tissue-specific phenotypes of DSCT, although further investigation of other cases of extra-abdominal DSCT is needed to confirm this speculation.

ACKNOWLEDGMENTS

The authors wish to thank Dr Jun-ichi Mimaya, Dr Shuzo Park, and Dr Chin-Ying Lo (Departments of Oncology, Plastic Surgery, and Ophthalmology, Shizuoka Children's Hospital) and Dr Nobutada Katori and Dr Yasuhisa Nakamura (Department of Oculoplastic Surgery, Seirei Hamamatsu General Hospital) for kindly contributing this case and providing the follow-up information. The authors also thank Mr Naoshi Ishikawa and Mr Motohiro Sano (Department of Clinical Pathology and Laboratory Medicine, Shizuoka Children's Hospital) for their excellent technical assistance.

REFERENCES

1 Swanson PE, Dehner LP, Wick MR. Polyphenotypic small cell tumors of childhood [Abstract]. *Lab Invest* 1988; **58**: 9.
2 May W, Gishizky ML, Lessnick S *et al.* Ewing sarcoma 11;22 translocation produces a chimeric transcription factor that requires the DNA-binding domain encoded by FLI1 for transformation. *Proc Natl Acad Sci USA* 1993; **90**: 5752–6.
3 Delattre O, Zucman J, Plougastel B *et al.* Gene fusion with an ETS DNA-binding domain caused by chromosome translocation in human tumours. *Nature* 1992; **359**: 162–5.

4 Urano F, Umezawa A, Yabe H et al. J. Molecular analysis of Ewing's sarcoma: Another fusion gene, EWS-E1AF, available for diagnosis. *Jpn J Cancer Res* 1998; **89**: 703–11.
5 Delattre O, Zuckman J, Melot T *et al.* The Ewing family of tumors: A subgroup of small-round-cell tumors defined by specific chimeric transcripts. *N Engl J Med* 1994; **331**: 294–9.
6 Adsay V, Cheng J, Athanasian E *et al.* Primary desmoplastic small cell tumor of soft tissues and bone of the hand. *Am J Surg Pathol* 1999; **23**: 1408–13.
7 Gerald WL, Miller HK, Battifora H *et al.* Intra-abdominal desmoplastic small round-cell tumor. Report of 19 cases of a distinctive type of high-grade polyphenotypic malignancy affecting young individuals. *Am J Surg Pathol* 1991; **15**: 499–513.
8 Ladanyi M, Gerald W. Fusion of the EWS and WT1 genes in the desmoplastic small round cell tumor. *Cancer Res* 1994; **54**: 2837–40.
9 Murray JC, Minifee PK, Trautwein LM *et al.* Intraabdominal desmoplastic small round cell tumor presenting as a gastric mural mass with hepatic metastases. *J Pediatr Hematol Oncol* 1996; **18**: 289–92.
10 Ordi J, de Alava E, Torne A *et al.* Intraabdominal desmoplastic small round cell tumor with EWS/ERG fusion transcript. *Am J Surg Pathol* 1998; **22**: 1026–32.
11 Slominski A, Wortzman J, Carlson A *et al.* Molecular pathology of soft tissue and bone tumors. *Arch Pathol Lab Med* 1999; **123**: 1246–59.
12 Bismar TA, Basturk O, Gerald WL *et al.* Desmoplastic small cell tumor in the pancreas. *Am J Surg Pathol* 2004; **28**: 808–12.
13 Young RH, Eichhorn JH, Dickersin GR *et al.* Ovarian involvement by the intraabdominal desmoplastic small round cell tumor divergent differentiation: A report of three cases. *Hum Pathol* 1992; **23**: 454–64.
14 Resnick MB, Donovan M. Intra-abdominal desmoplastic small round cell tumor with extensive extra-abdominal involvement. *Pediatr Pathol Lab Med* 1995; **15**: 797–803.
15 Cumming OW, Ulbright TM, Young RH *et al.* Desmoplastic small round cell tumors of the paratesticular region. *Am J Surg Pathol* 1997; **21**: 219–25.
16 Parkash V, Gerald WL, Parma A *et al.* Desmoplastic small round cell tumor of the pleura. *Am J Surg Pathol* 1995; **19**: 659–65.
17 Tison V, Cerasoli S, Morigi F *et al.* Intracranial desmoplastic small-cell tumor. Report of a case. *Am J Surg Pathol* 1996; **20**: 112–17.
18 Venkateswaran L, Jenkins JJ, Kaste SC *et al.* Disseminated intrathoracic desmoplastic small round-cell tumor: A case report. *J Pediatr Hematol Oncol* 1997; **19**: 172–5.
19 Antonescu CR, Gerald WL, Magid MS *et al.* Molecular variants of the EWS-WT1 gene fusion in desmoplastric small round cell tumor. *Diagn Mol Pathol* 1998; **7**: 24–8.
20 Gerald WL, Ladanyi M, de Alava E *et al.* Clinical, pathologic, and molecular spectrum of tumors associated with t(11;22)(p13;q12): Desmoplastic small round-cell tumor and its variants. *J Clin Oncol* 1998; **16**: 3028–36.
21 Hill DA, O'Sullivan MJ, Zhu X *et al.* Practical application of molecular genetic testing as an aid to the surgical pathologic diagnosis of sarcomas. A prospective study. *Am J Surg Pathol* 2002; **26**: 965–77.
22 De Alava E, Landanyi M, Rosai J *et al.* Detection of chimeric transcripts in desmoplastic small round cell tumor and related developmental tumors by reverse transcriptase polymerase chain reaction. A specific assay. *Am J Pathol* 1995; **147**: 1584–91.
23 Su MC, Jeng YM, Chu YC. Desmoplastic small round cell tumor of the kidney. *Am J Surg Pathol* 2004; **28**: 1379–83.
24 Shimizu Y, Mitsui T, Kawakami T *et al.* Novel breakpoint of the EWS gene and the WT1 gene in a desmoplastic small round cell tumor. *Cancer Genet Cytogenet* 1998; **106**: 156–8.

The Prostate 67:41–49 (2007)

Angiotensin II Type I Receptor Antagonist as An Angiogenic Inhibitor in Prostate Cancer

Takeo Kosaka,[1] Akira Miyajima,[3]* Eiji Takayama,[2] Eiji Kikuchi,[3] Jun Nakashima,[3] Takashi Ohigashi,[1] Tomohiko Asano,[1] Michiie Sakamoto,[4] Hajime Okita,[4] Masaru Murai,[3] and Masamichi Hayakawa[1]

[1]*Department of Urology, National Defense Medical College, Tokorozawa, Saitama, Japan*
[2]*Department of Parasitology, National Defense Medical College, Tokorozawa, Saitama, Japan*
[3]*Department of Urology, Keio University School of Medicine, Shinjuku-ku, Tokyo, Japan*
[4]*Department of Pathology, Keio University School of Medicine, Shinjuku-ku, Tokyo, Japan*

BACKGROUND. Angiotensin II (AII) type 1 receptor (AT1R) antagonists are used widely as antihypertensive agents, and long-term AT1R blockade may have a protective effect against cancer. We previously demonstrated that specific AT1R blockade with candesartan, an AT1R antagonist, inhibited vascular endothelial growth factor (VEGF) production and dramatically decreased lung metastasis of renal cancer by inhibiting tumor angiogenesis. This study was then undertaken to investigate the effects of AT1R blockade using candesartan in prostate cancer (PCa).

METHODS. We first determined whether hormone-independence is associated with tumor angiogenesis and AT1R expression. Accordingly, we postulated that AT1R blockade may affect angiogenesis in androgen-independent PCa rather than in androgen-dependent PCa, and investigated the effects of AII and candesartan on PCa cell lines and a tumor xenograft model.

RESULTS. A human hormone-refractory PCa (HRPC) and C4-2 androgen-independent PCa cell line showed significantly higher expression of VEGF, MVD, and AT1R than did human androgen-dependent PCa and an LNCaP androgen-dependent PCa cell line. In vitro, AII and candesartan did not directly affect the proliferation of LNCaP and C4-2 cells, but candesartan significantly suppressed VEGF production in C4-2 cells. In vivo, candesartan significantly suppressed VEGF expression, serum PSA concentration and tumor growth (1.1 ± 0.2, 45.0 ± 17.6 ng/ml, 235.8 ± 37.4 mm^3) in C4-2 xenografts in castrated mice, compared with the controls ($2.4 + 0.6$, $376.7 + 74.2$ ng/ml, $830.8 + 147.6$ mm^3).

CONCLUSIONS. Candesartan exerted preventive effects on HRPC, rather than on androgen-sensitive PCa, through the inhibition of tumor angiogenesis. *Prostate 67: 41–49, 2007.*

KEY WORDS: **prostate cancer; hormone; refractory; angiotensin II**

INTRODUCTION

Prostate cancer (PCa) is one of the most common malignancy in Western countries and is the second leading cause of cancer mortality in the United States. Currently, patients with advanced or metastatic PCa are treated by androgen ablation alone or in combined with local therapy. While hormonal ablation is the standard therapy for advanced PCa and most patients initially respond to androgen ablation, in more than 80% of the patients the tumor will subsequently acquire androgen independence [1] and the cancer ultimately becomes fatal [2]. To date, no treatments specifically effective for hormone-refractory prostate cancer

*Correspondence to: Akira Miyajima, MD, Department of Urology, Keio University School of Medicine, 35 Shinanomachi, Shinjuku-ku, Tokyo 160-8582, Japan. E-mail: akiram@sc.itc.keio.ac.jp
Received 16 March 2006; Accepted 19 May 2006
DOI 10.1002/pros.20486
Published online 16 October 2006 in Wiley InterScience (www.interscience.wiley.com).

(HRPC) are available, although a number of therapies have been tested.

Angiotensin II (AII) is a key biological peptide in the renin-angiotensin system that regulates blood pressure and renal hemodynamics. The two major AII receptors subtypes are AT1R and AT2R. AT1R belongs to the seven transmembrane domain superfamily, and its stimulation activates classical second messenger systems that lead to the rapid production of diacylglycerol and inositol 1,4,5-triphosphate as well as the activation of protein kinase C [3]. Nevertheless, AT1R is localized in not only cell membrane but also cytoplasm because of its internalization [4,5].

The potential tumor growth promoting effects of AII has been suspected based on its known hormonal actions and its vasoconstrictor effect [6]. It has been suggested that angiotensin-converting enzyme (ACE) inhibitors may offer protection against cancer and may prevent carcinogenesis [7]. Several studies have shown that AII can induce neovascularization in experimental systems [8] by way of AT1R [9]. AT1R is also frequently expressed in human tumors such as skin cancer [10], renal cell carcinoma [5,11], and breast cancer [12]. A recent in vitro study showed that treatment with an AT1R antagonist inhibited the growth of a pancreatic cancer cell line, suggesting that AT1R blockade may be a useful therapeutic strategy for cancer [4]. Candesartan was developed as a specific long-acting AT1R antagonist, and it has been widely used as an antihypertensive agent. We previously demonstrated that lung metastasis of murine renal cancer showed significant AT1R expression and that candesartan inhibited vascular endothelial growth factor (VEGF) production and dramatically decreased lung metastasis in a mouse model by inhibiting tumor angiogenesis [5], and confirmed anti-angiogenic effects in bladder cancer tumor xenograft model as well [13].

It is well known that angiogenesis is essential for tumor progression and metastasis [14–16]. In relation to PCa, it has also been suggested that the degree of tumor angiogenesis is related to clinical stage [17,18], progression after radical prostatectomy [19], and survival [20,21]. Various endothelial growth factors, namely, angiogenic factors produced by cancer cells, have been shown to play crucial roles in tumor angiogenesis. VEGF is one of the most potent and specific angiogenic factor. Immunohistochemical studies have shown that PCa cells produce VEGF [22,23], and that VEGF expression correlates with microvessel density (MVD) and tumor progression [24].

In this study, we hypothesized that AT1R blockade may have a therapeutic effect on PCa, if AT1R were involved in tumor angiogenesis in PCa. We then sought to investigate the expression of angiogenic factors and AT1R in PCa and tested the effects of AT1R blockade on PCa.

MATERIALS AND METHODS

Clinical Samples and Clinicopathological Features

Archival paraffin-embedded sections were obtained from 25 patients who underwent retropubic radical prostatectomy for localized PCa between January 2001 and December 2001. None of the patients had received hormonal treatment prior to the operation. The average age of the patients at the time of surgery was 64.0 ± 6.2 years. Gleason score was less than 7 in 14 patients and 7–10 in 10 patients. According to the TNM system, there were 16 patients in clinical stage II and 8 in stage III.

Twenty-four prostate specimens were also randomly selected from the archival paraffin-embedded sections of patients who had died of HRPC and had undergone autopsy in our institutions. The average age of these patients was 70.7 ± 11.8 years. The Gleason score of all 24 samples was more than 6 and clinically all of them were in stage IV. All these patients had been subjected to androgen ablation alone or to androgen ablation plus chemotherapy or radiation. Of them, two had a serum PSA level of less than 10 ng/ml; the others had levels of 10 ng/ml or higher. Histology of the specimens was evaluated by two independent pathologists using hematoxylin and eosin-stained slides.

It is impossible to prove that all the surgical specimens were androgen-dependent tumors. Nevertheless, more than 80% of the patients responded to the treatment at the beginning, thereafter they suffered a relapse and only 20% were well controlled for 5 years [25,26]. Accordingly, most of our patients who were not subjected to neoadjuvant androgen ablation may have had androgen-dependent tumors [27].

Murine Xenograft Prostate Cancer Model

LNCaP cells and C4-2 cells, an androgen-independent LNCaP subline [28], were grown in RPMI 1640 medium containing 10% fetal calf serum. Six-week-old male athymic nude BALB/C mice were castrated by scrotal incision under local anesthesia, and were used to create a xenograft model with C4-2 cells [28], while intact male athymic nude BALB/C mice were used to create a xenograft model with LNCaP cells. Twenty mice per group were subcutaneously inoculated with 5×10^6 cells suspended in 100 μl of Matrigel (Becton Dickinson Labware, Lincoln Park, NJ). The volume of the tumors was calculated using the formula: tumor volume (mm^3) = length × width × height × 0.52. When the tumor volume reached 80–100 mm^3, the animals were killed and the subcutaneous tumors were harvested. In the AT1R administration model, the treatment was started on Day 1. Tumors were measured every 4 days. The serum concentration of PSA

was determined using an enzymatic immunoassay kit (MEDICORP, Montreal, Canada).

Immunostaining for CD34, VEGF, and AT1R

Formalin-fixed paraffin-embedded sections (4 μm) were deparaffinized, rehydrated, and washed in PBS. Endogenous peroxidase was quenched. A blocking step was included using 1% bovine serum albumin in conjunction with avidin and biotin blocking solutions. The tissue section were overlaid with the primary antibody (anti-CD34 monoclonal antibody, Nichirei, Tokyo, Japan; anti-VEGF polyclonal antibody, Neo-Markers, Freemont, CA, anti-AT1R polyclonal antibody, Santa Cruz Biotechnology Inc, Santa Cruz, CA) and incubated at 4°C overnight. After incubation with a biotinylated secondary antibody, the tissue sections were incubated with avidin-biotin peroxidase complex, and color was developed with diaminobenzidine. After washing the slides, they were counter-stained with 10% hematoxylin for 1–2 min. MVD was assessed in areas of the tumor containing the highest numbers of microvessels using the criteria established by Weidner et al. [17]. Briefly, individual microvessels were counted on a ×200 field under a light microscope. Any CD34-positive endothelial cell or cell cluster that was clearly separated from adjacent microvessels, tumor cells, and other connective tissue elements was considered a single, countable microvessel. MVD was calculated by the number of microvessels per 1 mm^2. A computer-driven microscopic scanner, MacScope (MITANI Corp, Fukui, Japan) was used. The intensity of AT1R and VEGF staining in tumor lesions was graded on a scale of 0 to +3, with 0 indicating no detectable staining and +3 indicating the strongest staining. Immunopositivity of tumor lesions for VEGF was assessed in all lesions at a high power (×400) by two independent investigators operating in a blinded fashion [5].

Immunocytochemistry

For immunocytochemistry, PCa cells were grown on glass coverslips and the cells were fixed with acetone for 15 min. The cells were then washed and incubated with an anti-AT1R rabbit polyclonal antibody (Santa Cruz Biotechnology). After washing with PBS, they were incubated for 1 hr with FITC-labeled anti-rabbit IgG. The coverslips were washed with PBS, mounted on glass slides and viewed under a confocal laser-scanning microscope.

Effects of AT1R Blockade In Vitro

LNCaP (10^4) or C4-2 (10^4) cells were plated in 96-well plates and allowed to attach at 37 C in a humidified atmosphere of 5% CO_2/95% O_2 for 24 hr. After the medium was replaced with serum free medium for 4 hr, the cells were incubated with AII or CV11974, which is the active form of candesartan, at various concentrations between 10^{-9} and 10^{-5} M for 24, 48, or 72 hr. At the end of the incubation period, ^{3}H-thymidine incorporation assay was performed to determine the effects of AII and candesartan on LNCaP and C4-2 cells.

ELISA Assay for VEGF in Conditioned Medium

Cells were seeded in 60 mm^2 dishes and allowed to attach at 37 C in a humidified atmosphere of 5% CO_2/95% O_2. After 24 hr, the medium was replaced with serum free medium for 4 hr, and then the cells were incubated with conditioned medium (AII 10^{-8} M or candesartan 10^{-7} M, or AII 10^{-8} M and candesartan 10^{-7} M). After 24 hr (C4-2, LNCaP) or 6 hr (C4-2), the supernatant was collected and VEGF was measured using commercially available ELISA kits (Quantikine, R&D Systems, Minneapolis, MN). The protein level for VEGF was quantified by comparing its optical density to the standard curve for VEGF and normalizing it for the cell number.

Statistical Analysis

All results were analyzed for statistical significance by the ANOVA or chi-square test. Data are expressed as the mean value ± SEM. The level of significance was set at $P < 0.05$. Statistical analysis was performed using Statview 5.0 software (SAS Institute, Cary, NC).

RESULTS

MVD, VEGF and AT1R Expression in Human Prostate Cancer

The specimens from patients with HRPC showed a significantly higher MVD (65.1 ± 6.3, Fig. 1B) than the surgical specimens from patients without androgen ablation (35.3 ±2.7, $P < 0.01$, Fig. 1A). In all the samples (Table I), MVD was closely associated with a higher Gleason score (≥7). This finding was consistent with previous observations of prostate biopsy samples and metastatic PCa specimens [17,20,29]. We next investigated whether hormone independence was related to VEGF expression by immunostaining the specimens for VEGF. HRPC samples showed a significantly higher VEGF expression (1.9 ± 0.6, n = 24, $P < 0.01$, Fig. 1D), than the surgical specimens from patients without androgen ablation (0.8 ± 0.4, n = 25, Fig. 1C).

As for AT1R expression, this was mainly detected in tumor vessels and tumor cells. HRPC samples showed significantly higher AT1R expression (1.5 ± 0.3, n = 24, $P < 0.01$, Fig. 1F) than the surgical specimen from

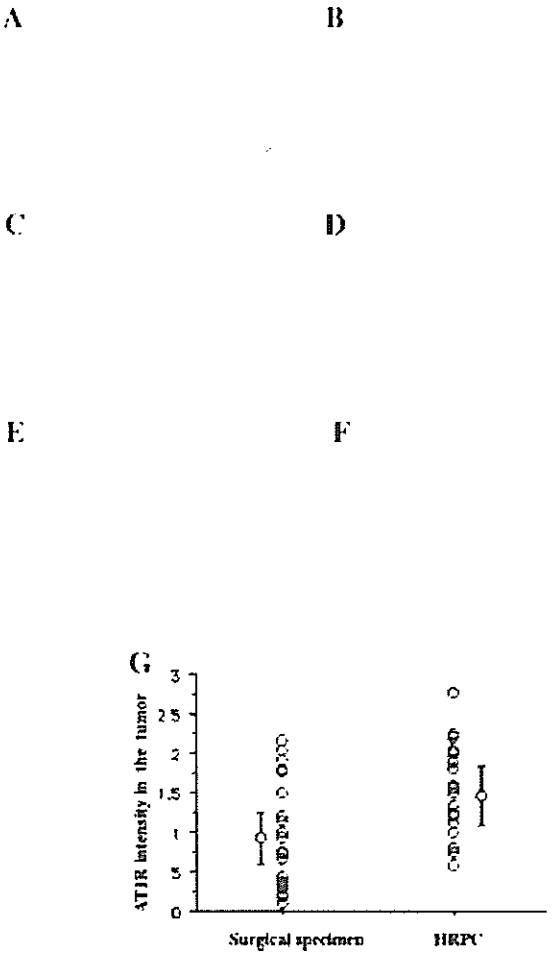

Fig. 1. Serial photo panels showing HRPC (**B, D, F**) and surgical specimens (**A, C, E**). Immunohistochemical staining for CD34 (A, B), VEGF (C, D) and ATIR (E, F) expression in PCa is shown. Magnification is 1:200. **G**: Intensity of ATIR expression in human specimens by distribution by dot plot.

patients without androgen ablation (0.9 ± 0.3, n = 25, Fig. 1E), as shown in Figure 1G.

ATIR Expression In Vitro

We also investigated AT1R expression in androgen-sensitive LNCaP cells and androgen-independent C4-2 cells by immunocytochemistry. Although both cell lines expressed AT1R, C4-2 cells (Fig. 2A) showed a significantly higher AT1R expression than LNCaP cells (Fig. 2B).

TABLE I. Different Expression Pattern of MVD in Surgical Specimen and HRPC

	Gleason score		Stage	
	5–6	7–10	I + II	III + IV
MVD < 50	13	14	13	14
MVD ≥ 50	1	21	3	19
	$P < 0.05$			NS

Mice Xenograft Model

We next evaluated the angiogenic parameters in a mouse xenograft model using immunohistochemical techniques. The MVD of C4-2 tumors in castrated mice (14.0 ± 1.6, n = 9, $P < 0.01$, Fig. 3A) was also significantly higher than that of LNCaP tumors (7.7 ± 1.2, n = 6, Fig. 3B). C4-2 tumors in castrated mice showed significantly higher VEGF expression (2.4 ± 0.6, n = 9, $P = 0.004$, Fig. 3C) than LNCaP tumors (1.1 ± 0.2, n = 6, Fig. 3D). These results suggest that neovascularization is more aggressively induced in HRPC. In addition, both LNCaP and C4-2 tumors showed a prominent AT1R expression, with C4-2 tumors exhibiting a significantly higher AT1R expression (2.0 ± 0.3, n = 5, $P < 0.0001$, Fig. 3E) than LNCaP tumors (0.4 ± 0.2, n = 6, Fig. 3F). These findings indicated that the HRPC primary lesion was characterized by a significantly higher VEGF production and neovascularization than androgen-dependent PCa.

ATIR Antagonist Administration to the Mice Xenograft Model

The above results suggested that targeting tumor angiogenesis through AT1R may be a possible treatment for HRPC. To test this hypothesis, we orally administered candesartan (10 mg/kg) to nude mice bearing a C4-2 tumor. Candesartan treatment resulted in a dramatic decrease in the volume of subcutaneous tumor nodules and serum PSA concentration in the treated group (235.8 ± 37.4 mm^3, $P < 0.01$; 45.0 ± 17.6 ng/ml, $P < 0.01$) compared to the untreated group (830.8 ± 147.6 mm^3; 376.7 ± 74.2 ng/ml; Fig. 4A) at Day 28. To evaluate tumor neovascularization, we immunostained tissue samples using a CD34 monoclonal antibody. The MVD of the subcutaneous tumors in the control group was 14.0 ± 4.8 (Fig. 4B). Candesartan significantly decreased tumor MVD in the treated group (5.9 ± 0.8, $P < 0.001$, Fig. 4C). Investigation of VEGF expression showed that tumors treated with candesartan exhibited a significantly lower VEGF expression (1.6 ± 0.4, Fig. 4E) than tumors not treated with candesartan (2.3 ± 0.5, $P < 0.01$, Fig. 4D). We performed the same experiments in nude mice bearing a LNCaP tumor for 6 weeks. In this case, however, candesartan had no significant effects on LNCaP tumors growth (data not shown).

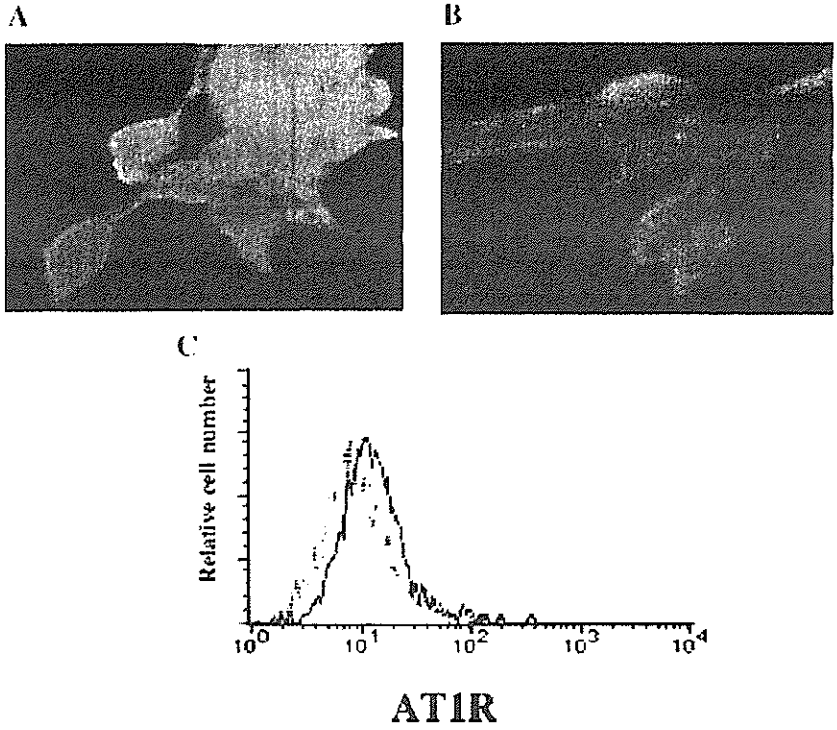

Fig. 2. ATIR expression was demonstrated by immunocytochemistry. **A**: C4-2, **B**: LNCaP. Magnification is 1:200. **C**: ATIR expression detected in C4-2 cells and LNCaP cells by FACS. Solid line: C4-2 cells, dotted line: LNCaP cells.

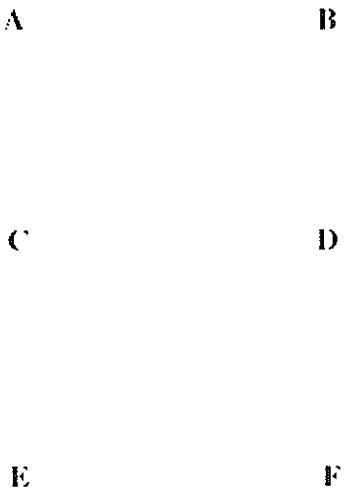

Fig. 3. Serial photo-panels showing immunohistochemical staining for C4-2 tumors (**A**,**C**,**E**) and LNCaP tumors (**B**,**D**,**F**). Immunohistochemical staining for CD34 (A, B), VEGF (C, D), and ATIR (E, F). Magnification is 1:200.

Effects of ATIR Blockade by Candesartan on DNA Synthesis In Vitro

To examine AII-induced effects on cell growth, LNCaP and C4-2 cells were incubated with increasing concentrations of the active form of the AT1R antagonist (CV11974) or AII for 24 hr (Fig. 5A,B). Neither CV11974 nor AII affected the proliferation of these cell lines (LNCaP, C4-2) at any of the concentrations tested. Similar results were observed at 48 and 72 hr. In vitro proliferation assay at clinically achievable concentration of AII (10^{-9}–10^{-8}) and CV11974 (10^{-8}–10^{-7}) showed no effect on cell proliferation.

VEGF Secretion From PCa Cells

In humans and mice, HRPC expresses significantly more VEGF than hormone-dependent PCa. We therefore sought to assess VEGF production in PCa cells. In C4-2 cells, VEGF production was significantly higher (9.8 ± 1.5 pg/10^3 cells, $n = 5$, $P < 0.001$) than in LNCaP cells (2.3 ± 0.3 pg/10^3 cells, $n = 5$) at the 24-hr timepoint. At the 6-hr timepoint, VEGF production was also detected in C4-2 cells (2.2 ± 0.4 pg/10^3 cells, Fig. 6). AII stimulated VEGF production in C4-2 cells (4.5 ± 0.2 pg/10^3 cells, $n = 5$, $P = 0.01$), while CV11974 significantly inhibited AII-induced VEGF production in these cells